

## ASTROMETRY AND SPATIO-KINEMATICS OF H<sub>2</sub>O MASERS IN THE MASSIVE STAR-FORMING REGION NGC 6334I(NORTH) WITH VERA

JAMES O. CHIBUEZE<sup>1,2</sup>, TOSHIHIRO OMODAKA<sup>3</sup>, TOSHIHIRO HANDA<sup>3</sup>, HIROSHI IMAI<sup>3</sup>, TOMOHARU KURAYAMA<sup>4</sup>,  
TAKUMI NAGAYAMA<sup>5</sup>, KAZUYOSHI SUNADA<sup>5</sup>, MAKOTO NAKANO<sup>6</sup>, TOMOYA HIROTA<sup>5</sup>, AND MAREKI HONMA<sup>5</sup>

<sup>1</sup> East Asian ALMA Regional Center, National Astronomical Observatory of Japan, 2-21-1 Osawa, Mitaka, Tokyo 181-8588, Japan; james.chibueze@nao.ac.jp

<sup>2</sup> Department of Physics and Astronomy, Faculty of Physical Sciences, University of Nigeria, Carver Building, 1 University Road, Nsukka, Nigeria

<sup>3</sup> Department of Physics and Astronomy, Graduate School of Science and Engineering, Kagoshima University, 1-21-35 Korimoto, Kagoshima 890-0065, Japan

<sup>4</sup> Center for Fundamental Education, Teikyo University of Science, 2525 Yatsusawa, Uenohara, Yamanashi 409-0193, Japan

<sup>5</sup> Mizusawa VLBI Observatory, National Astronomical Observatory of Japan, 2-21-1 Osawa, Mitaka, Tokyo 181-8588, Japan

<sup>6</sup> Faculty of Education and Welfare Science, Oita University, Oita 870-1192, Japan

*Received 2013 August 22; accepted 2014 February 5; published 2014 March 12*

### ABSTRACT

We measured the trigonometric parallax of an H<sub>2</sub>O maser source associated with the massive star-forming region NGC 6334I(North), hereafter as NGC 6334I(N), with the VLBI Exploration of Radio Astrometry. The derived annual parallax is  $0.789 \pm 0.161$  mas, corresponding to a distance of  $1.26^{+0.33}_{-0.21}$  kpc. Using the new distance, we recalculated the physical parameters (masses and luminosities) of the dust continuum cores in the region, and the revised parameters are only  $\sim 50\%$  of their originally reported values. We also traced 23 relative proper motions of the H<sub>2</sub>O masers associated with SMA1 (central millimeter source in the region) between epochs, which exhibit an average amplitude of maser proper motion of  $\sim 2.03$  mas yr<sup>-1</sup> ( $\sim 12.22$  km s<sup>-1</sup>), tracing a bipolar outflow. The bipolar outflow structure extends through  $\sim 600$  mas ( $\sim 720$  AU), with a dynamical timescale of  $\sim 295$  yr. Using an expanding flow model, we derived the most plausible dynamical center of the outflow, pointing to SMA1b (1.3 cm and 7 mm continuum source) as the outflow driving source. Based on our results and other existing parallax results, we derive the pitch angles of the Sagittarius arm as  $6^{\circ}2 \pm 5^{\circ}4$  along the Galactic longitude range of  $\sim 0^{\circ}7 - \sim 40^{\circ}1$  assuming a perfect logarithmic spiral. We derived the peculiar motion of NGC 6334I(N) to be  $-4 \pm 1$  km s<sup>-1</sup> toward the Galactic center,  $8 \pm 2$  km s<sup>-1</sup> in the direction of the Galactic rotation, and  $25 \pm 2$  km s<sup>-1</sup> toward the Galactic north pole.

*Key words:* astrometry – stars: distances – stars: individual (NGC 6334IN)

### 1. INTRODUCTION

Measurement of the distances to massive star-forming regions is necessary for diagnosing their physical conditions/properties such as luminosity, masses, sizes, and studying the evolution of the young stellar and/or proto-stellar objects. The widely used kinematic distance from the Sun to a source in the Milky Way is derived from the radial velocity of the source and the galactic rotation model. There is a high risk of significant difference among the photometric, kinematic and actual distances if their photometric magnitudes are affected by interstellar extinction and if their motions are affected in one way or the other by nearby supernovae or super-bubble or the gravitational potentials of the spiral arm and/or the galactic bar (e.g., Foster et al. 2012). There are very long baseline interferometry (VLBI) observation reports showing significant difference in the parallactic and kinematic distances to some sources due to large peculiar motions of the source influenced by an expanding super-bubble (e.g., Sato et al. 2008), a gravitational perturbations from the galactic bar (Brunthaler et al. 2009), an expanding arm effect (Sanna et al. 2009), and other factors (e.g., Kurayama et al. 2011).

VLBI Exploration of Radio Astrometry (VERA) is especially dedicated to phase-referencing VLBI observations with the aim of measuring the annual parallaxes of galactic maser sources whose results were recently summarized by Honma et al. (2012). Equipped with a dual-beam system (Honma et al. 2008), VERA is able to simultaneously observe a maser source and a position reference (quasar) source, thus improving its effectiveness in phase-referencing observations. VLBI observation of the masers

and gas kinematics also trace activities associated with the formation of high mass stars. Spatio-kinematics of masers can be used to describe the three-dimensional (3D) motion of individual masing cloudlets (1–300 AU size) around massive young stellar objects (MYSOs). These maser proper motions can trace periodic violent ejections from the central star, collimated bipolar outflows and wide-angle outflows (e.g., Torrelles et al. 2011; Chibueze et al. 2012; Goddi et al. 2006).

NGC 6334I(N) is a massive star-forming region located on the northeast of the molecular cloud/H II region complex NGC 6334 (an optical emission nebula popular called Cat's Paw nebula), which is expected to be located in the Sagittarius-Carina arm (hereafter referred to as Sagittarius arm), based on its photometric distance by Neckel (1978). The complex extends  $32' \times 40'$  across the sky. In the literature, the widely accepted distance to NGC 6334 is  $1.74 \pm 0.31$  kpc, obtained via photometric measurements (Neckel 1978), while the rarely used kinematic distance is  $0.7 \pm 1.9$  kpc (Wilson et al. 1970). Considering the outdated assumptions used in the kinematic distance calculations, we examined a recent model by Reid et al. (2009) and recalculated the kinematic distance using the local standard of rest velocities ( $V_{\text{LSR}}$ ) reported in Wilson et al. (1970) and Brogan et al. (2009). The obtained values in the order of (associated source, kinematic distance,  $V_{\text{LSR}}$ , source of the  $V_{\text{LSR}}$  value) are (SMA1, 0.87 kpc,  $-3.2$  km s<sup>-1</sup>, H109 $\alpha$  velocity from Table 1 of Wilson et al. 1970), (SMA1, 1.03 kpc,  $-4$  km s<sup>-1</sup>, H109 $\alpha$  velocity from Table 4 of Wilson et al. 1970), (SMA1, 0.67 kpc,  $-2.2$  km s<sup>-1</sup>, H109 $\alpha$  velocity from Table 5 of Wilson et al. 1970), (SMA1, 0.83 kpc,  $-3$  km s<sup>-1</sup>; Brogan et al. 2009), and (SMA2, 1.21 kpc,  $-5$  km s<sup>-1</sup>; Brogan et al. 2009).

**Table 1**  
VERA Observations of NGC 6334I(N)

Code	Observation Epoch	JVN Telescopes <sup>a</sup>	VERA Astrometry?
r10037a	2010 Feb 6	VERA, NICT, Gifu	Yes <sup>b</sup>
r10137a	2010 May 17	VERA, NRO	No
r10316a	2010 Nov 12	VERA, NICT	No
r11060b	2011 Mar 1	VERA	Yes
r11110a	2011 Apr 20	VERA, NRO	Yes
r11139a	2011 May 19	VERA, NRO	No
r11273a	2011 Sep 30	VERA	Yes
r11299a	2011 Oct 26	VERA	Yes
r12065a	2012 Mar 5	VERA, NRO	Yes
r12097b	2012 Apr 6	VERA, NRO	Yes

#### Notes.

<sup>a</sup> Telescopes that participated in the epoch of observation. VERA comprises of Mizusawa, Iriki, Ogasawara, and Ishigakijima stations. NICT is the National Institute of Communication Technology 34 m telescope Kashima, while NRO represents Nobeyama Radio Observatory 45 m telescope. Gifu is an 11 m telescope in northern Japan.

<sup>b</sup> This epoch was not used in the annual parallax fitting.

Noticeably, the derived kinematic distances are dependent on the accuracy of the  $V_{LSR}$ , supposing all other parameters and assumptions are correct. The distance of 1.21 kpc obtained for the SMA2 object of NGC 6334I(N) is similar to the parallax distance we have derived (see Section 4.1). NGC 6334I(N) is the least evolved cluster protostars in the complex (less evolved than NGC 6334I), both separated by  $90''$  and shows different characteristics (Beuther et al. 2005). NGC 6334I(N) contains multiple millimeter objects, most of which show evidence of ongoing star formation activity (Hunter et al. 2006; Brogan et al. 2009). Sandell (2000) reported the size, gas mass, and bolometric luminosity of NGC 6334I(N) to be  $\sim 10''$  (0.08 pc),  $\sim 400 M_{\odot}$ , and  $\sim 1.9 \times 10^3 L_{\odot}$ , respectively, assuming a distance of 1.74 kpc (Neckel 1978). In this paper, we report the results of the measurement of trigonometric parallax (with VERA only), and the relative proper motions of  $H_2O$  masers associated with NGC 6334I(N) (with Japanese VLBI Network, JVN, consisting of VERA and other radio telescopes in Japan).

## 2. OBSERVATIONS

The observations of the  $H_2O$  ( $6_{15-5_{23}}$ ) masers in NGC 6334I(N) at a rest frequency of 22.235080 GHz were carried out in 10 epochs spanning about 2 yr from 2010 February 6 to 2012 April 6 (see Table 1 for the details of the observation epochs) using JVN. The JVN observations comprised of VERA, Nobeyama 45 m, National Institute of Communications Technology (NICT) Kashima 34 m, Gifu 11 m (only the first epoch) telescopes. VERA only was used for the annual parallax measurement, while VERA along with NRO, and NICT, which provided added sensitivity was used for measuring the relative proper motions of the water masers. Using the dual-beam system of the VERA telescopes, the  $H_2O$  masers of NGC 6334I(N) and a position-reference source J1713–3418 were simultaneously observed. J1713–3418 belongs to the Very Long Baseline Array (VLBA < Galactic Plane Survey catalog by Petrov et al. (2011), with a positional uncertainty of 0.44 mas in right ascension (R.A.) and 0.92 mas in declination. These two sources are spatially separated by  $1'.44$ . At each epoch, the total observation time was about 5 hr, including the scans on NGC 6334I(N),

a bandpass calibrator (NRAO 530), and the position-reference source, J1713–3418. The data were recorded onto magnetic tapes at the rate of 1024 Mbps, providing a total bandwidth of 256 MHz, which were digitized in four quantization levels and then divided into 16 base-band channels (BBCs) with a bandwidth of 16 MHz each. One of the BBCs was assigned to the  $H_2O$  maser emission in NGC 6334I(N), while the remaining 15 BBCs were assigned to the continuum emission from the position-reference source.

The data correlation was made with the Mitaka FX correlator. The accumulation period of the correlation was set to 1 s. The correlation outputs consisted of 512 and 32 spectral channels for the  $H_2O$  maser and reference continuum emission, respectively. The  $H_2O$  maser spectral resolution was 15.625 kHz, corresponding to a velocity spacing of  $0.42 \text{ km s}^{-1}$ .

## 3. DATA REDUCTION

The two-beam astrometric data reduction was conducted with the VERA Data Analyzer (VEDA) developed by the software development group at the Mizusawa VLBI Observatory of the National Astronomical Observatory of Japan for astrometric analysis of VERA data (Niinuma et al. 2011). We adopted the following phase tracking centers for the observed sources; J1713–3418 (position-reference source) ( $\alpha_{J2000} = 17^{\text{h}}13^{\text{m}}09^{\text{s}}.941507$  and  $\delta_{J2000} = -34^{\circ}18'29''.4276$ ) and NRAO 530 (bandpass calibrator) ( $\alpha_{J2000} = 17^{\text{h}}33^{\text{m}}02^{\text{s}}.70579$  and  $\delta_{J2000} = -13^{\circ}04'49''.54823$ ). The reference position of NGC 6334I(N) was set as ( $\alpha_{J2000} = 17^{\text{h}}20^{\text{m}}55^{\text{s}}.192$  and  $\delta_{J2000} = -35^{\circ}45'03''.77$ , corresponding to Galactic longitude,  $l$ , and latitude,  $b$  of  $351^{\circ}.45$  and  $0^{\circ}.66$ , respectively) in a recalculation of the delay tracking model.

The VEDA pipeline data reduction steps include time and frequency averaging (Niinuma et al. 2011) of the position-reference source, J1713–3418, to reduce the size of the data set. System-temperature ( $T_{\text{sys}}$ )-based amplitude calibration and bandpass calibration of NGC 6334I(N) (target maser source), and J1713–3418 were performed with the total-power spectra of the bandpass calibrator (NRAO 530). The delay and delay-rate offset were determined by a fringe search process on NRAO 530. The station solutions determined by NRAO 530 were used in the fringe search of J1713–3418, after which the image were obtained by CLEAN deconvolution and then self-calibration was performed on the obtained image. The phase solutions of J1713–3418, obtained with integration time of 1 s, was applied to the maser source to obtain its absolute position. The typical peak intensity of J1713–3418 was  $\sim 270 \text{ mJy beam}^{-1}$ . Doppler tracking was carried out on the maser source. The velocity channels containing bright maser spots were imaged with a field of view of  $2'' \times 2''$  with  $1024 \times 1024$  grids in order to find maser spots detected at a signal-to-noise ratio over 5. The final images of individual detected maser spots were obtained each with an area of  $10 \text{ mas} \times 10 \text{ mas}$  (size) with  $512 \times 512$  grids.

The single-beam, self-calibrated imaging of the  $H_2O$  masers in NGC 6334I(N) was done with Astronomical Image Processing System (AIPS) package developed by the National Radio Astronomy Observatory (NRAO), using the standard procedures. The instrumental delay calibration was carried out with the scans on the calibrator, NRAO 530. The fringe fitting and self-calibration procedures were performed for a Doppler shifted channel including a bright and quasi-consistent maser spot (velocity component) in the SMA1 region of NGC 6334I(N). Their solutions were applied to all the data and then the map of the maser clusters were made. The CLEAN deconvolved

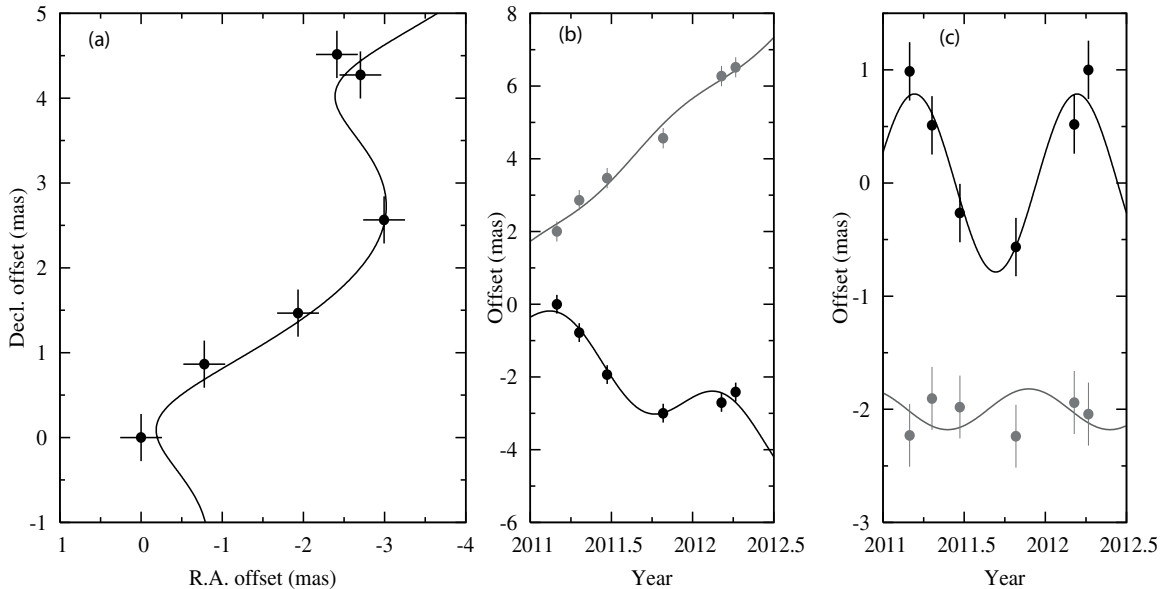


**Figure 1.** (a) Maser feature position on the sky and the modeled maser motion (solid curve). (b) Maser feature position in R.A. (black circle) and decl. (gray circle) offsets against the epoch of observation. (c) Same as (b) but a linear proper motion is subtracted. The error bars are estimated as explained in Section 4.

image cubes of the maser source were created using the beam that was synthesized from naturally weighted visibilities. The typical synthesized beam size was  $\sim 1.3$  milliarcseconds (mas). The  $\text{H}_2\text{O}$  maser image cubes were made with a cell size of 0.2 mas. For the wide-field mapping and objective maser spot identification, we used an automatic pipeline script which runs on the AIPS POPS environment and mainly consists of AIPS tasks and adverbs: IMAGR, IMSTAT, and SAD. The  $\text{H}_2\text{O}$  maser spot identification was done by adopting a signal-to-noise ratio cut-off of  $\sim 7$ . From the Gaussian fitting errors, we estimated the accuracies of the relative positions of the maser spots to be 0.01–0.30 mas in R.A. and 0.02–0.30 mas in declination. The individual maser features were defined as clusters of maser spots or velocity components and each feature position was defined from the brightness peak of the feature following the identification method of Imai et al. (2002), also used in Chibueze et al. (2012). We used the results of our astrometric analysis to determine the absolute position of the masers and adopted a reference position for superimposing the maser maps.

## 4. RESULTS

### 4.1. Annual Parallax of NGC 6334I(N)

We typically detected an average of  $\sim 30$  maser spots per epoch and one reasonably stable maser spot of local standard of rest velocity ( $v_{\text{LSR}}$ )  $-10.1 \text{ km s}^{-1}$  was detected in 70% of all the observation epochs. The  $v_{\text{LSR}}$  range of the detected maser spots is  $-23 \text{ km s}^{-1}$  to  $3 \text{ km s}^{-1}$ , distributed over an area of  $400 \text{ mas} \times 400 \text{ mas}$ . The detected maser features (a group of maser spots coincident at the same position and velocity) were highly variable and extended so as to be resolved out in VERA longer baselines like the Mizusawa–Ishigakijima baseline. As such, we have discretely selected significantly compact maser emissions from the  $-10 \text{ km s}^{-1}$  component for annual parallax measurement to improve its accuracy. Finally, we decided to use only the  $-10 \text{ km s}^{-1}$  maser feature detected in seven epochs for the annual parallax fitting. Only six out of the seven epochs were used for the parallax fitting. This is because the maser feature was detected in the first epoch (observation code r10037a) and

**Table 2**  
Results of the Parallax Fitting for NGC 6334I(N)

$v_{\text{LSR}}$ ( $\text{km s}^{-1}$ )	$\mu_{\alpha} \cos \delta^a$ ( $\text{mas yr}^{-1}$ )	$\mu_{\delta}^b$ ( $\text{mas yr}^{-1}$ )	Parallax ( $\pi$ ) (mas)
10.1	$-2.20 \pm 0.26$	$3.93 \pm 0.28$	$0.79 \pm 0.16$

#### Notes.

<sup>a</sup> Proper motion of the maser spot in the right ascension direction. The Galactic longitude,  $l$ , and latitude of the NGC 6334I(N) are  $b$  of  $351^\circ 45'$  and  $0^\circ 66'$ , respectively.

<sup>b</sup> Proper motion of the maser spot in the declination direction.

subsequently in the fourth epoch with a space of 1 yr non-detection period. In fitting the annual parallax the first epoch data point clearly deviated from the fit, thus, was not used in the annual parallax measurement. The feature detected in the first epoch is most likely different from that detected later though they have the same velocity.

We obtained the annual parallax ( $\pi$ ) to be  $0.789 \pm 0.161$  mas, corresponding to a distance of  $1.26_{-0.21}^{+0.33}$  kpc with 20% accuracy. The standard deviations of the post-fit residuals were 0.238 and 0.278 mas in R.A. and declination, respectively. We introduced an error floor of 0.238 mas and 0.278 mas in R.A. and declination, respectively, for all of the results of the position measurements to make the reduced  $\chi^2$  to be unity in the least-squares analysis. These error floors can be defined as the positional uncertainties in the astrometric observations that may have originated from the difference in the optical path lengths between the target and reference sources, caused by the atmospheric zenith delay residual and/or a variability of the structure of the maser feature (Honma et al. 2007; Hirota et al. 2007).

Figure 1 shows the positions of the maser spot used for the parallax fitting and absolute proper motion fittings. The positional variations show systematic sinusoidal modulation with a period of 1 yr, caused by the parallax. Table 2 shows the parallax fitting results and the obtained absolute proper motion of the maser spot. Our obtained parallax distance to NGC 6334I(N) is  $\sim 500$  pc less than the photometric distance (Neckel 1978) but is very similar to the recalculated kinematic

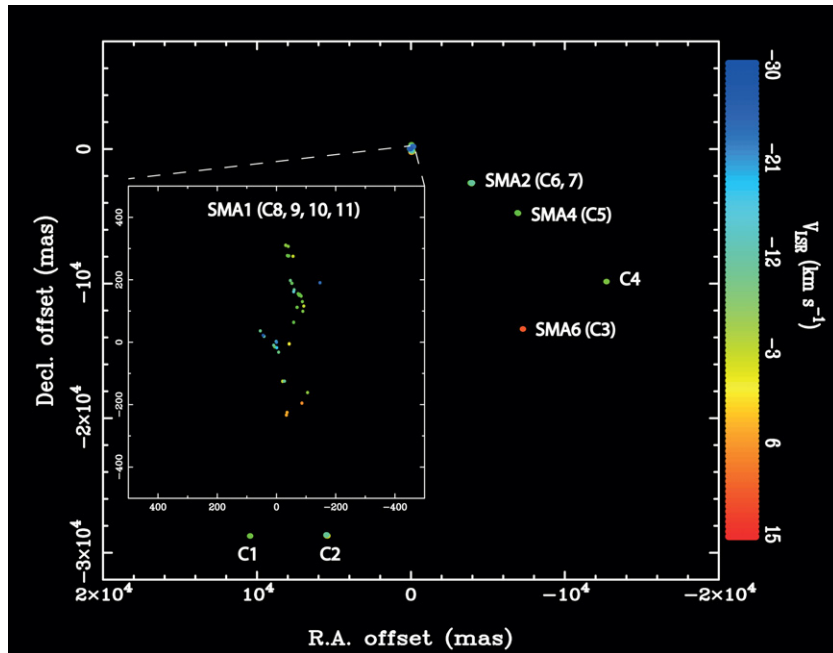


**Figure 2.** Distribution of all the H<sub>2</sub>O maser clusters and features detected in observations toward NGC 6334I(N). Insert: zoom of the H<sub>2</sub>O maser distribution associated with the SMA1 object. The reference maser position is located at R.A.(J2000.0) = 17<sup>h</sup>20<sup>m</sup>55<sup>s</sup>.1909, decl.(J2000.0) = -35°45′03″.7987.

distance using Reid’s model (Reid et al. 2009), and the  $V_{\text{LSR}}$  of SMA2 from Brogan et al. (2009; see Section 1).

The dust and gas mass estimates of millimeter cores are strongly dependent on the source distance. Recently, Sandell (2000) and Brogan et al. (2009) estimated the dust and gas mass associated with individual objects detected toward NGC 6334I and I(N). In both cases, the mass calculations were made with the distance of 1.7 kpc (Neckel 1978), therefore, we revised the mass and luminosity estimates in Sandell (2000) and Brogan et al. (2009) using our parallax distance of 1.26 kpc as a benchmark (see Table 3). The originally reported values are reduced by 50%, and this cast some doubt on the ability of some of the millimeter continuum cores to evolve into massive stars.

#### 4.2. H<sub>2</sub>O Maser Distribution and Spatio-kinematics in SMA1 Object of NGC 6334I(N)

We detected H<sub>2</sub>O maser clusters corresponding to C1 to C11, some associated with millimeter objects. However, others are not associated with any millimeter source as previously reported by Brogan et al. (2009) in one of the observation epochs carried out under the best weather and other observation conditions (including usage of large antennas). A total of  $\sim 200$  maser features were detected in our observations. Figure 2 shows the distribution of the H<sub>2</sub>O maser clusters detected in our JVN observation on 2010 May 17. Because the self-calibration procedure, using a bright maser spot in SMA1, was applied in order to also detect weak maser emissions, all the map origin represents the location of SMA1. Our astrometric data reduction was used to determine the absolute position of the reference bright maser spot to be  $(\alpha, \delta)_{\text{J2000}} = (17^{\text{h}}20^{\text{m}}55^{\text{s}}.1909, -35^{\circ}45′03″.7987)$  on 2010 May 17 within 1 mas error. This error is a combination of the errors due to the residual phase in phase-referencing, the zenith delay of the troposphere and the ionosphere, the instrumental offset calibration, and the low declination nature of the target source. Using this reference position, we have investigated the correspondence of each maser cluster with the results of Brogan et al. (2009). Figure 2 (insert) shows the distribution of the H<sub>2</sub>O

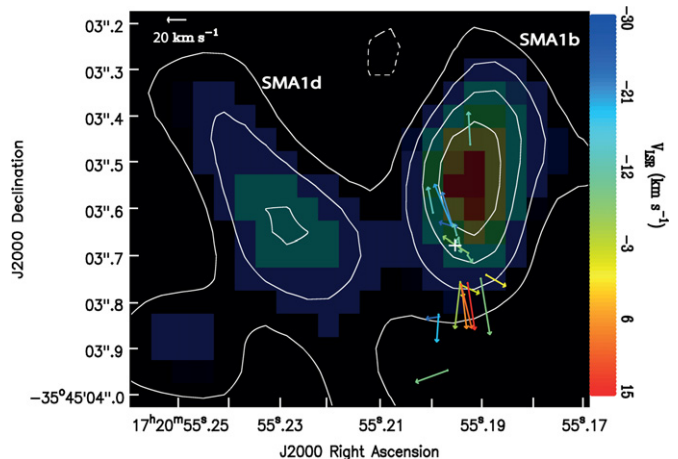


**Figure 3.** Proper motions of the H<sub>2</sub>O maser spots relative to the brightest spot derived from our observations superposed on the zoomed 1.3 cm continuum with VLA (Brogan et al. 2009; Rodríguez et al. 2007) in white contours with pseudo color. The synthesized beam and the rms noise of the image are  $0''.38 \times 0''.27$  and  $64 \mu\text{Jy beam}^{-1}$ . The contour levels are  $-0.0954, 0.0954, 0.191, 0.286,$  and  $0.382 \text{ mJy beam}^{-1}$ . The vectors show the position (start point of the vector) and relative proper motion on the sky, respectively. The white plus symbol at  $(\alpha, \delta)_{\text{J2000}} = (17^{\text{h}}20^{\text{m}}55^{\text{s}}.1909, -35^{\circ}45′03″.70)$  shows the most probable location of the driving source from the observed maser kinematics (see Section 4.2).

maser features in SMA1 object. The other maser clusters are likely tracing star formation activities in the region especially those associated with millimeter sources.

Figure 3 shows the traced relative proper motions of 23 H<sub>2</sub>O maser features (traced in three or more adjacent epochs with the criteria that the feature must be identical in  $V_{\text{LSR}}$ , and position; see Table 4) in SMA1 (consisting of four 1.3 cm continuum objects, SMA1a, b, c (Rodríguez et al. 2007) and 1d reported by Brogan et al. 2009) object of NGC 6334I(N) overlaid on the zoomed Very Large Array (VLA) 1.3 cm continuum image of the compact SMA1b and 1d objects around the

**Table 3**  
Revised Physical Parameters of NGC 6334I(N)

Source	Recalculation of the Masses and Luminosities Reported Sandell (2000) and Brogan et al. (2009)						
	Values Reported	Revised Values			1.3 mm Core	Values Reported	Revised Values
	(Sandell 2000)	$M_{\text{tot}}^a$	$L_{\text{tot}}^a$	$M_{\text{tot}}$	$L_{\text{tot}}$	(Brogan et al. 2009)	$M_{\text{gas}}^a$
	( $M_{\odot}$ )	( $L_{\odot}$ )	( $M_{\odot}$ )	( $L_{\odot}$ )		( $M_{\odot}$ )	( $M_{\odot}$ )
NGC 6334I	200	$2.6 \times 10^5$	106	$1.38 \times 10^5$	SMA1	16–14	9–7
SM1	175	$1.2 \times 10^3$	93	$0.64 \times 10^3$	SMA2	7–6	4–3
SM2	70	$1.2 \times 10^3$	37	$0.64 \times 10^3$	SMA3	74–23	39–12
SM3	100	$0.4 \times 10^3$	53	$0.21 \times 10^3$	SMA4	52–16	28–9
NGC 6334I(N)	400	$1.9 \times 10^3$	212	$1.01 \times 10^3$	SMA5	28–9	15–5
SM4	120	$0.4 \times 10^3$	64	$0.21 \times 10^3$	SMA6	32–13	17–7
SM5	120	$0.4 \times 10^3$	64	$0.21 \times 10^3$	SMA7	22–7	12–4
SM6	100	$0.2 \times 10^3$	53	$0.11 \times 10^3$			
SM7	130	$0.4 \times 10^3$	69	$0.21 \times 10^3$			
SM8	80	$0.2 \times 10^3$	42	$0.11 \times 10^3$			

**Note.** <sup>a</sup> Sandell (2000) and Brogan et al. (2009) estimations were based on the distance of 1.74 kpc (Neckel 1978).

**Table 4**  
Relative Proper Motions of the Water Maser in SMA1 Object of NGC 6334I(N)

Feature	Offset		Proper Motion				Radial Motion	
	R.A.	Decl.	$\mu_x$	$\sigma \mu_x$	$\mu_y$	$\sigma \mu_y$	$V_{\text{LSR}}$	$\Delta V_{\text{LSR}}$
1	17.17	30.26	-1.41	3.48	0.26	4.25	-28.96	2.42
2	17.19	31.41	3.82	1.87	1.00	4.20	-25.67	1.58
3	53.52	-191.32	3.85	0.28	-0.53	0.99	-23.47	3.16
4	18.32	33.85	2.93	1.95	8.57	4.83	-21.08	1.58
5	20.12	32.93	4.98	2.97	10.81	5.19	-19.68	0.84
6	56.00	-186.31	0.54	1.38	-7.13	3.17	-18.29	1.37
7	71.79	64.85	1.48	1.62	6.67	3.19	-12.81	0.84
8	5.49	9.26	0.85	0.39	2.81	0.67	-12.32	1.26
9	-32.33	233.50	0.53	1.48	8.45	3.45	-12.05	0.62
10	-0.18	2.62	1.11	0.05	-1.14	0.07	-11.76	0.20
11	0.00	0.00	0.00	0.47	0.00	0.53	-11.32	1.26
12	0.00	0.01	-0.73	0.05	-3.39	0.28	-10.18	0.16
13	-24.92	-39.57	-1.35	1.66	-1.77	0.74	-9.86	0.94
14	31.08	-324.22	9.37	0.22	-3.04	1.41	-8.81	0.73
15	-62.00	-97.46	-2.69	1.53	-14.65	4.35	-8.32	0.37
16	-26.84	-34.25	7.40	0.19	4.22	0.60	-6.91	0.20
17	-4.51	-105.95	1.58	2.84	-12.15	5.53	-4.82	1.15
18	-4.16	-111.88	-5.59	2.94	-2.28	8.39	-1.37	0.73
19	-5.27	-108.93	-0.81	2.82	-3.51	6.80	-0.58	0.74
20	-77.29	-88.16	-5.71	1.52	-2.91	4.04	1.16	0.16
21	-8.13	-113.02	-1.51	3.67	-11.40	6.17	7.28	0.84
22	-6.55	-111.70	-3.19	2.01	-11.48	4.40	9.77	1.68
23	-25.30	-108.31	-2.09	2.86	-12.22	4.95	14.66	1.26

masing region. It is important to note that the 1.3 cm continuum image of Brogan et al. (2009) is what we used in this paper, was obtained from the reanalyzed data of Rodríguez et al. (2007). While the position accuracy of the VLA continuum object is estimated to be about 50 mas, VERA astrometric result provides maser feature absolute position accuracy better than 1 mas. The maser distribution is elongated along the north-south direction, extending over  $\sim 600$  mas ( $\sim 720$  AU) and tracing a bipolar outflow coincident with the position of SMA1b and may be associated with the outflow reported by Rodríguez et al. (2007). The mean proper motion amplitude of the maser features was obtained to be  $2.03 \text{ mas yr}^{-1}$  and all the observed maser proper motion most likely originated from the same driving source, except for the two features at  $(\alpha, \delta)_{\text{J2000}} = (17^{\text{h}}20^{\text{m}}55^{\text{s}}.197, -35^{\circ}45'03''.96)$  with

$v_{\text{LSR}} = -9 \text{ km s}^{-1}$  and  $(17^{\text{h}}20^{\text{m}}55^{\text{s}}.198, -35^{\circ}45'03''.82)$  with  $v_{\text{LSR}} = -25 \text{ km s}^{-1}$ . The driving source is most likely located at, or near, R.A. (J2000.0) =  $17^{\text{h}}20^{\text{m}}55^{\text{s}}.1909$ , and declination (J2000.0) =  $-35^{\circ}45'03''.70$  (see Figure 3) and is suggestive of a bipolar outflow driving source, associated with SMA1b. The dynamical timescale of the observed bipolar outflow activities is derived, from a half length of the maser feature distribution divided by the mean proper motion amplitude, to be  $\sim 295$  yr. This is in the same order as the dynamical timescale of the maser bipolar outflow activity associated with the Cepheus A HW3d of dynamical timescale ( $\sim 100$  yr; Chibueze et al. 2012) and some other episodic maser events (Torrelles et al. 2011).

To find the possible origin of the outflow, we performed least-squares fitting analysis following the same procedure reported in Imai et al. (2000, 2011) and Chibueze et al. (2012).

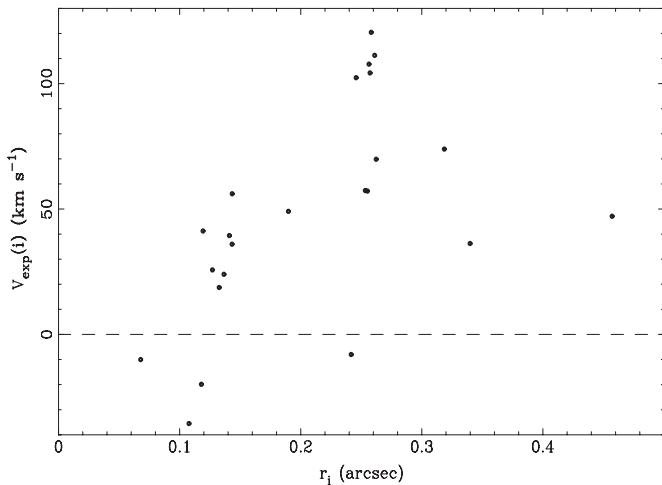


**Figure 4.** Expansion velocity distribution of the maser features in SMA1 object of NGC 6334I(N) derived from the model fitting (Section 4.2). The maximum error in  $V_{\text{exp}}(i)$  and  $r_i$  are  $\pm 4 \text{ km s}^{-1}$  and  $\pm 1 \text{ mas}$ , respectively. Below the dashed line ( $0 \text{ km s}^{-1}$  expansion velocity line) are the negative expansion velocities which could be explained misidentified proper motions and/or turbulence.

We adopted the radial velocity of the reference maser feature to be  $-12 \text{ km s}^{-1}$ . The number of maser features with measured proper motions,  $N_m$ , is 23. We first considered the 3D position vectors of the maser features with respect to the originating point of the outflow by assuming that the individual maser features are moving independently and radially from the originating point. The free parameters of the model fitting are the position vector of the originating point ( $x_0, y_0$ ) and the systemic motion vector of the outflow on the sky ( $V_{0x}, V_{0y}$ ).  $z_0 \equiv 0$  and  $V_{0z} = V_{\text{LSR}} = -12 \text{ km s}^{-1}$  are fixed.

The results of the model fitting is shown in Table 5, and the obtained dynamical center is also derived in the absolute coordinates within reasonable errors as shown in Figure 3.

Figure 4 shows the distributions of the derived maser expansion velocities, with the originating point considered to be close to the map origin (0,0) mas in offsets. With the assumed radial flow from an originating point, a positive and a negative expansion velocity means an outflow and an infall motion, respectively. All except four of the maser features exhibited positive expansion velocities with possible acceleration from 50 to  $100 \text{ km s}^{-1}$ . The negative expansion velocity components might be associated with turbulent motions or misidentification of the proper motions of the associated maser features.

## 5. DISCUSSION

### 5.1. Distance and Peculiar Motion of NGC 6334I(N)

We have determined the position, parallax, and proper motion of NGC 6334I(N) and its corresponding distance. Figure 5 shows that NGC 6334I(N) is most likely associated with gas belonging to the Sagittarius arm, following the spiral arm model by Russeil (2003).

From our expanding flow model, we estimated the proper motion of the reference maser spot with respect to the central object to be  $4.1 \pm 2.0 \text{ km s}^{-1}$ , and  $4.2 \pm 4.0 \text{ km s}^{-1}$  in the R.A. and declination, respectively. It is important to note that the absolute mean value of all the relative proper motions traced in SMA1b is  $3.5 \pm 9.9 \text{ km s}^{-1}$ , and  $-11.7 \pm 17.5 \text{ km s}^{-1}$  in R.A. and declination. We deduced the proper motion of the reference maser spot (of our model) from the absolute proper motion derive from our parallax fitting and computed

**Table 5**  
Parameters of the Best Fit 3D Spatio-kinematical Model of the H<sub>2</sub>O Masers in NGC 6334I(N)

Parameter	Value
$\Delta X_0$ (mas) <sup>a</sup>	$0 \pm 5$
$\Delta Y_0$ (mas) <sup>a</sup>	$-12 \pm 8$
$V_{0X}$ ( $\text{km s}^{-1}$ ) <sup>a</sup>	$4.1 \pm 2$
$V_{0Y}$ ( $\text{km s}^{-1}$ ) <sup>a</sup>	$4.2 \pm 4$
$V_{\text{LSR}}$ ( $\text{km s}^{-1}$ ) <sup>b</sup>	$-12$
$D$ (kpc) <sup>b</sup>	$1.26$
$\sqrt{\chi^2}$ <sup>c</sup>	$10.18$

**Notes.**

<sup>a</sup> Relative value respect to the maser feature ID 12.

<sup>b</sup> Adopted  $V_{\text{LSR}}$  of the reference maser feature.

<sup>c</sup> The  $\chi^2$ -square value was obtained in the model fitting based on the least-squares method.

the average of the summed value of the errors. The resultant motion, which we used for the peculiar motion calculation, is  $-2.88 \pm 0.30 \text{ mas yr}^{-1}$  and  $3.23 \pm 0.39 \text{ mas yr}^{-1}$  corresponding to  $-17.34 \pm 1.78 \text{ km s}^{-1}$ , and  $19.46 \pm 92.34 \text{ km s}^{-1}$  at 1.26 kpc, respectively.

We used the line-of-sight velocity of the central millimeter object of NGC 6334I(N), SMA1, ( $\sim -2.8 \pm 0.5 \text{ km s}^{-1}$  measured by Brogan et al. 2009 using  $\sim 5''$  scale compact millimeter line, CH<sub>3</sub>OH). Thus, we could convert positions and velocities of NGC 6334I(N) from the equatorial heliocentric reference frame to the Galactic reference frame following the procedure of Reid et al. (2009). We assumed a flat rotation of the Galactic frame. The distance of the Sun from the Galactic center ( $R_0$ ) and the rotation speed of the local standard of rest ( $\Theta_0$ ) were adopted as 8.05 kpc and  $235 \text{ km s}^{-1}$ , respectively (Honma et al. 2012). The standard solar motion,  $(U_{\odot}, V_{\odot}, W_{\odot}) = (11.10 \pm 0.75, 12.24 \pm 0.47, 7.25 \pm 0.37) \text{ km s}^{-1}$ , was adopted from Schonrich et al. (2010).

We derived the peculiar motion of NGC 6334I(N) to be  $(U_{\text{src}}, V_{\text{src}}, W_{\text{src}}) = (-4 \pm 1, 8 \pm 2, 25 \pm 2) \text{ km s}^{-1}$ , where  $U_{\text{src}}$ ,  $V_{\text{src}}$ , and  $W_{\text{src}}$  are directed toward the Galactic center, in the direction of Galactic rotation and toward the Galactic north pole, respectively. We compared our derived peculiar motion of NGC 6334I(N) with those reported in other sources (listed in Sakai et al. 2012) and found the obtained values to be similar (within the error values) to those of other regions located in the Sagittarius arm. Figure 5 shows the location of NGC 6334I(N) at 1.26 kpc (red filled circle), and 1.74 kpc (blue filled circle). The red arrow represents the resultant velocity ( $8.94 \pm 2.24 \text{ km s}^{-1}$ ) of NGC 6334I(N) in the galactic plane, derived from  $(U_{\text{src}}$ , and  $V_{\text{src}}$ ). The peculiar motion of NGC 6334I(N) toward the Galactic center and in the direction of Galactic rotation are in agreement with the values reported on source star-forming regions in the Sagittarius arm (see Sakai et al. 2012), but the motion toward the Galactic north pole is significantly larger than usual. There is a noticeable galactic north–south evolution of massive stars in the NGC 6334 complex (Rodríguez et al. 1982), which is also visible in the optical and infrared bands. We suggest that the overall star formation activities in the complex may be responsible for the observed high peculiar motion of NGC 6334I(N) toward the Galactic north pole.

### 5.2. Pitch Angle of Sagittarius Arm

The pitch angle of the Sagittarius arm has been a source of recent debate. Sato et al. (2010a) derived the pitch

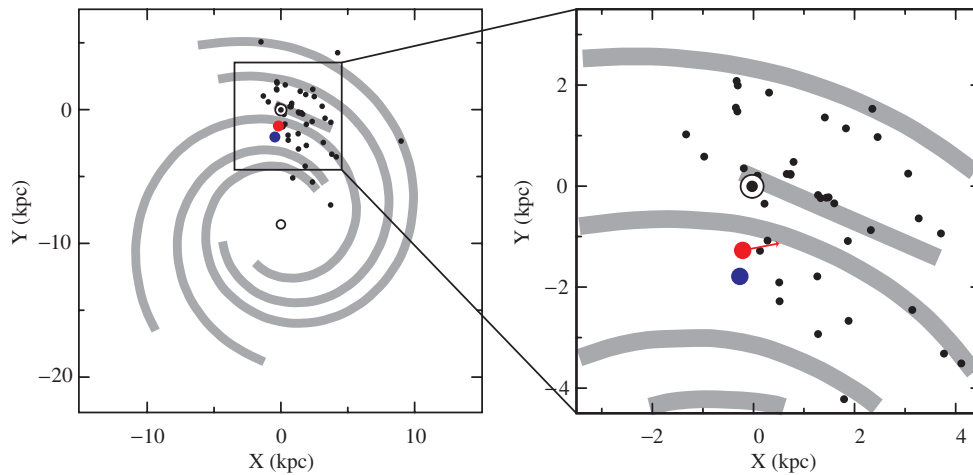


**Figure 5.** Positions of the sources (black filled circles) reported by Honma et al. (2012; annual parallaxes of the source have been measured) on Galactic plane. Location of the NGC 6334I(N) indicated by the red filled circle (this work), the red arrow indicates the peculiar motion of the source, and blue filled circle (based on 1.74 kpc; Neckel 1978). The spiral arms are depicted based on the Russeil (2003) arm model.

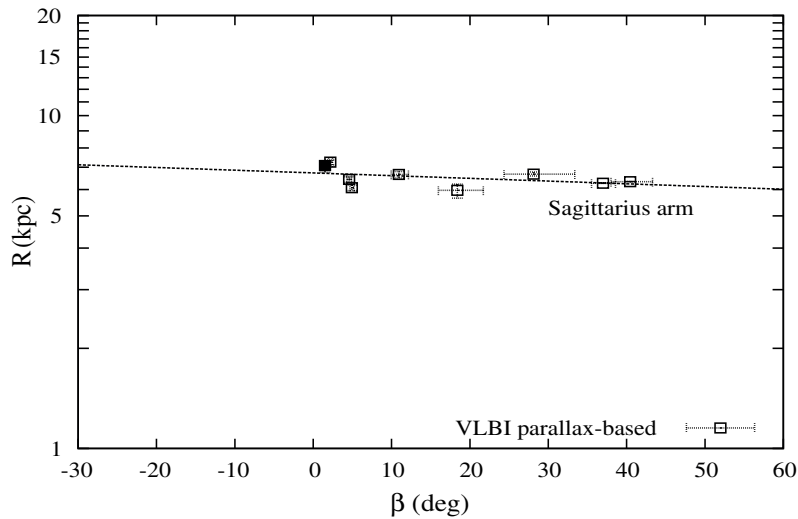


**Figure 6.** Fits of the pitch angle of the Sagittarius arm using sources in the arm with known parallax distance and NGC 6334I(N) indicated by the filled box (error estimates lie within the box).

angle,  $i$ ,<sup>7</sup> of the Sagittarius arm using the annual parallax results of G14.33–0.64 (Sato et al. 2010a), G35.20–0.74, G35.20–1.74 (Zhang et al. 2009), and W51 IRS2 (Xu et al. 2009). Sato et al. (2010a) fitted for the pitch angle ( $i$ ) of the Sagittarius arm using two possible combinations of three out of the four sources. They obtained ( $i$ ) to be  $11^{\circ}2 \pm 10^{\circ}5$  for a combination of G14.33–0.64, G35.20–0.74, and W51 IRS2, and  $34^{\circ}7 \pm 2^{\circ}7$  for G14.33–0.64, G35.20–0.74, and G35.20–1.74. Xu et al. (2013) obtained the pitch angle of the Local Arm to be  $10^{\circ}1 \pm 2^{\circ}7$ , which based on private communication reported in Xu et al. (2013) is similar to those of the Sagittarius and Perseus arm from their unpublished BeSSeL results: [www3.mpif-bonn.mpg.de/staff/abrunthaler/BeSSeL/index.shtml](http://www3.mpif-bonn.mpg.de/staff/abrunthaler/BeSSeL/index.shtml). They argued that it is not a spur (not a bifurcate of the Sagittarius arm as suggested by Sato et al. 2010a) but could be a branch that is closer to the Perseus arm than to the Sagittarius arm.

Assuming a perfect logarithmic spiral, we derive the pitch angle of the Sagittarius arm using our results, NGC 6334I(N), and other available parallax results (IRAS 19213 (Oh et al.

2010), W51 Main/South (Sato et al. 2010b), G48.61+0.02 (Nagayama et al. 2011), G35.20–0.74 & G35.20–1.74 (Zhang et al. 2009), G12.89+0.49 & G15.03–0.68 (Xu et al. 2011), G14.33–0.64 (Sato et al. 2010a)), which covers a Galactic longitude range of  $\sim 0^{\circ}7 - \sim 40^{\circ}1$ . We estimated the pitch angle to be  $6^{\circ}2 \pm 5^{\circ}4$  (see Figure 6), which is similar to the pitch angle of the Local Arm reported by Xu et al. (2013). For a comparison, we tried to fit the pitch angle of the Sagittarius arm excluding NGC 6334I(N) and obtained  $4^{\circ}2 \pm 5^{\circ}9$ . More results from both the BeSSeL and VERA projects will be needed to better constrain the pitch angle of the Sagittarius arm.

## 6. SUMMARY AND CONCLUSIONS

We made multi-epoch JVN (including VERA) observations toward NGC 6334I(N) at  $\sim 22$  GHz ( $H_2O$  maser frequency). We measured the trigonometric annual parallax of the  $H_2O$  maser source associated with NGC 6334I(N) to be  $0.789 \pm 0.161$  mas, which corresponds to a distance of  $1.26^{+0.33}_{-0.21}$  kpc. Since our measured distance is  $\sim 500$  pc less than the widely used 1.74 kpc (Neckel 1978), we revised the physical parameters of the region.

We derived the pitch angle of the Sagittarius arm as  $6^{\circ}2 \pm 5^{\circ}4$ . We derived the peculiar motion of NGC 6334I(N) to be  $-4 \pm 1$  km  $s^{-1}$  toward the Galactic center,  $8 \pm 2$  km  $s^{-1}$  in the

<sup>7</sup> The angle between the arm and the tangent of the Galactocentric circular orbit, expressed as  $\ln(R/R_{\text{ref}}) = -(\beta - \beta_{\text{ref}}) \tan i$ , where  $R$  is the Galactocentric radius at a Galactocentric longitude  $\beta$ ; see Sato et al. (2010a) and Reid et al. (2009).

direction of the Galactic rotation, and  $25 \pm 2 \text{ km s}^{-1}$  toward the Galactic north pole. We suggested that the star formation activities in the entire NGC 6334 complex could be responsible for the observed peculiar motion of I(N) toward the Galactic north pole.

The structure of the maser proper motions trace a bipolar outflow, and the average proper motion velocity is  $\sim 2.03 \text{ mas yr}^{-1}$  corresponding to  $\sim 12.22 \text{ km s}^{-1}$ . This suggests the expansion of the masing cloudlets powered by a central source. In an effort to study the proper motion in other maser clusters in the region, we are exploring archive data from other observational wavelengths for more information about the exciting sources in the region. High-resolution continuum observation of the exciting source with JVLA and ALMA will be necessary to extract the physical parameters of the MYSO.

We thank the anonymous referee for constructive comments and suggestions, which has helped improve the quality of this paper. We appreciatively acknowledge support of staff members of VERA project and the Astrophysics group of Kagoshima University. Our heartfelt appreciation goes to the students who have played some role in the VERA array operation at the four stations. J.O.C. has been financially supported for most part of this work by the Ministry of Education, Culture, Sports, Science, and Technology of Japan. We are also grateful to Crystal Brogan (NRAO) for providing us with the VLA 1.3 cm image of NGC 6334I(N).

## REFERENCES

- Beuther, H., Thorwirth, S., Zhang, Q., et al. 2005, *ApJ*, **627**, 834  
 Brogan, C. L., Hunter, T. R., Cyganowski, C. J., et al. 2009, *ApJ*, **707**, 1  
 Brunthaler, A., Reid, M. J., Menten, K. M., et al. 2009, *ApJ*, **693**, 424  
 Chibueze, J. O., Imai, H., Tafuya, D., et al. 2012, *ApJ*, **748**, 146  
 Foster, J. B., Stead, J. J., Benjamin, R. A., Hoare, M. G., & Jackson, J. M. 2012, *ApJ*, **751**, 157  
 Goddi, C., Moscadelli, L., Torrelles, J. M., Uscanga, L., & Cesaroni, R. 2006, *A&A*, **447**, L9  
 Hirota, T., Bushimata, T., Choi, Y. K., et al. 2007, *PASJ*, **59**, 897  
 Honma, M., Bushimata, T., Choi, Y. K., et al. 2007, *PASJ*, **59**, 889  
 Honma, M., Kijima, M., Suda, H., et al. 2008, *PASJ*, **60**, 935  
 Honma, M., Nagayama, T., Ando, K., et al. 2012, *PASJ*, **64**, 136  
 Hunter, T. R., Brogan, C. L., Megeath, S. T., et al. 2006, *ApJ*, **649**, 888  
 Imai, H., Kameya, O., Sasao, T., et al. 2000, *ApJ*, **538**, 751  
 Imai, H., Omi, R., Kurayama, T., et al. 2011, *PASJ*, **63**, 1293  
 Imai, H., Watanabe, T., Omodaka, T., et al. 2002, *PASJ*, **54**, 741  
 Kurayama, T., Nakagawa, A., Sawada-Satoh, S., et al. 2011, *PASJ*, **63**, 513  
 Nagayama, T., Omodaka, T., Handa, T., et al. 2011, *PASJ*, **63**, 719  
 Neckel, T. 1978, *A&A*, **69**, 51  
 Niinuma, K., Nagayama, T., Hirota, T., et al. 2011, *PASJ*, **63**, 9  
 Oh, C. S., Kobayashi, H., Honma, M., et al. 2010, *PASJ*, **62**, 101  
 Petrov, L., Kovalev, Y. Y., Fomalont, E. B., & Gordon, D. 2011, *AJ*, **142**, 35  
 Reid, M. J., Menten, K. M., Zheng, X. W., et al. 2009, *ApJ*, **700**, 137  
 Rodríguez, L. F., Canto, J., & Moran, J. M. 1982, *ApJ*, **255**, 103  
 Rodríguez, L. F., Zapata, L. A., & Ho, P. T. P. 2007, *ApJL*, **654**, L143  
 Russeil, D. 2003, *A&A*, **397**, 133  
 Sakai, N., Honma, M., Nakanishi, H., et al. 2012, *PASJ*, **64**, 108  
 Sandell, G. 2000, *A&A*, **358**, 242  
 Sanna, A., Reid, M. J., Moscadelli, L., et al. 2009, *ApJ*, **706**, 464  
 Sato, M., Hirota, T., Honma, M., et al. 2008, *PASJ*, **60**, 975  
 Sato, M., Hirota, T., Reid, M. J., et al. 2010a, *PASJ*, **62**, 287  
 Sato, M., Reid, M. J., Brunthaler, A., & Menten, K. M. 2010b, *ApJ*, **720**, 1055  
 Schonrich, R., Binney, J., & Dehnen, W. 2010, *MNRAS*, **403**, 1829  
 Torrelles, J. M., Patel, N. A., Curiel, S., et al. 2011, *MNRAS*, **410**, 627  
 Wilson, T. L., Mezger, P. G., Gardner, F. F., & Milne, D. K. 1970, *A&A*, **6**, 364  
 Xu, Y., Li, J. J., Reid, M. J., et al. 2013, *ApJ*, **769**, 15  
 Xu, Y., Moscadelli, L., Reid, M. J., et al. 2011, *ApJ*, **733**, 25  
 Xu, Y., Reid, M. J., Menten, K. M., et al. 2009, *ApJ*, **693**, 413  
 Zhang, B., Zheng, X., Reid, M. J., et al. 2009, *ApJ*, **693**, 419